19th AIAA Computational Fluid Dynamics
22 - 25 June 2009, San Antonio, Texas

AIAA 2009–4273

An Assessment of Dual-Time Stepping, Time Spectral and Artificial Compressibility based Numerical Algorithms for Unsteady Flow with Applications to Flapping Wings

Antony Jameson
Department of Aeronautics and Astronautics
Stanford University, Stanford, CA 94305-3030
Sriram
Schenectady, NY

19th AIAA Computational Fluid Dynamics
Jun 22-25, 2009/San Antonio, TX

An Assessment of Dual-Time Stepping, Time Spectral and Artificial Compressibility based Numerical Algorithms for Unsteady Flow with Applications to Flapping Wings

Antony Jameson*
Department of Aeronautics and Astronautics
Stanford University, Stanford, CA 94305-3030
Sriram†
Schenectady, NY

Summary

The objective of this study is to compare and contrast three numerical algorithms that can be used to estimate the forces and pressure distribution on wings in flapping motion. All algorithms are used to solve the unsteady Navier-Stokes equations in two dimensions at low Reynolds Numbers. The four algorithms are a) an A-stable, implicit discretization b) the time-spectral algorithm that implicitly assumes that the flow-field in temporally periodic, c) incompressible formulations of a) and d) incompressible formulations of b) using the artificial compressibility method. The methods in a) and b) have been reported earlier in literature but their application to flapping wing flows at low Reynolds number is new. The algorithms introduced in c), and d) are new and previously not reported in literature. In this abstract, the four algorithms are used for roughly similar test cases to obtain preliminary estimates for their merits and demerits. The final version of the paper will use the same test case for all the algorithms to enable even-handed comparison of the different numerical methods.

Background

Insect flight control has been studied extensively from a physiological perspective, but its mechanics are not understood well. Even when the kinematic changes elicited by a given stimulus have been defined, their consequences for aerodynamic force production often remain obscure. Quasi-steady aerodynamics have been largely supplanted by unsteady theories and is widely accepted as the mechanism that leads to the forces produced by insects in flight.[3,4] Lighthill[1] performed some of the earliest theoretical studies on the aerodynamics of insect flight shows the variation of lift and drag as observed by Weis-Fogh and Jensen.[2] A variety of experimental studies have enabled a better understanding of the nature of wing articulation by insects in hover and forward flight. While these studies enabled the authors to propose a variety of possible theories for insect flight, the lack of a complete understanding of the flight control mechanisms have prevented a more comprehensive understanding of insect flight control. It is not clear how many degrees of freedom an insect controls to enable it to perform its various maneuvers. Further, insects in controlled laboratory environments tend to produce lift and drag forces that are different from those observed in nature leading one to look for alternate analysis tools. It is also difficult to replicate subtle shifts in the center-gravity or even get a good estimate of the center of gravity of the insect that further clouds our understanding. Finally, there is a wide body of evidence that suggests that unlike conventional aircrafts/flight vehicles the control inputs for insects are highly non-orthogonal that complicates the process of separating the various motions. This ability of insects is interesting for both practical and theoretical studies because it might provide us with clues to develop more efficient control mechanisms for conventional aircraft.

Fast and Efficient Numerical Solution Techniques

To obtain accurate and fast estimates of the forces produced during the flapping motion, one needs to efficiently integrate the Navier-Stokes equations in time. The dual time stepping scheme provides a convenient formulation for a fully implicit scheme for true unsteady flows. To exploit the periodic nature of the flow over insect wings, alternate techniques need to be developed. Finally, the low speed nature of the flows, requires efficient modification of the numerical algorithms to alleviate the stiffness introduced by disparate eigenvalues of the governing system of equations.

In the following subsections, the four numerical methods we explore are detailed.

*Thomas V. Jones Professor of Engineering, Stanford University
†Technology Philanthropist

Implicit Schemes for Unsteady Flow using the Backward Difference Formula (BDF)

Time dependent calculations are needed for a number of important applications, such as flutter analysis, or the analysis of the flow past a helicopter rotor, in which the stability limit of an explicit scheme forces the use of much smaller time steps than would be needed for an accurate simulation. In this situation, the fast steady state solvers can be used to obtain a converged solution at each time step of an implicit scheme.[9]

Suppose that the semi-discrete form of the governing equations is approximated as

$$D_t w^{n+1} + R(w^{n+1}) = 0. \tag{1}$$

Here $R(w)$ is the spatial discretization of the flux terms and D_t is a k^{th} order accurate backward difference operator of the form

$$D_t = \frac{1}{\Delta t} \sum_{q=1}^{k} \frac{1}{q} (\Delta^-)^q, \tag{2}$$

where

$$\Delta^- w^{n+1} = w^{n+1} - w^n.$$

Applied to the linear differential equation

$$\frac{dw}{dt} = \alpha w$$

the schemes with $k = 1, 2$ are stable for all $\alpha \Delta t$ in the left half plane (A-stable). Dahlquist has shown that A-stable linear multi-step schemes are at best second order accurate.[10] Gear however, has shown that the schemes with $k \leq 6$ are stiffly stable,[11] and one of the higher order schemes may offer a better compromise between accuracy and stability, depending on the application.

Dual Time-Stepping method with the BDF

Equation (1) along with a choice of the time discretization operator (2) can now treated as a modified steady state problem to be solved by a multigrid scheme using variable local time steps in a fictitious time t^*. For example, in the case of the second order BDF one solves

$$\frac{\partial w}{\partial t^*} + R^*(w) = 0,$$

where

$$R^*(w) = \frac{3}{2\Delta t} w + R(w) - \frac{2}{\Delta t} w^n + \frac{1}{2\Delta t} w^{n-1},$$

and the last two terms are treated as fixed source terms. In previous work the multigrid scheme has been implemented using a modified Runge Kutta (RK) method, in which the convective and diffusive terms are treated separately in order to expand the stability region. The first term in the modified residual $R^*(w)$ shifts the Fourier symbol of the equivalent model problem to the left in the complex plane. While this promotes stability, it may also require a limit to be imposed on the magnitude of the local time step Δt^* relative to that of the implicit time step Δt. This may be relieved by a point-implicit modification of the multi-stage scheme.[12] In the case of problems with moving boundaries the equations must be modified to allow for movement and deformation of the mesh.

This method has proved effective for the calculation of unsteady flows that might be associated with wing flutter[13,14] and also in the calculation of unsteady incompressible flows.[15] It has the advantage that it can be added as an option to a computer program which uses an explicit multigrid scheme, allowing it to be used for the efficient calculation of both steady and unsteady flows.

If the inner iterations required to converge the solution at each time step are small, the dual time-stepping method is an efficient A-stable scheme that allows large steps to be taken by the numerical simulation. However, if a large number of inner iterations are required at each step, then the method becomes expensive. Moreover, it is hard to access the accuracy of the scheme unless the inner iterations are fully converged.

Time Spectral Methods[7]

There are many unsteady flows in engineering devices such as turbomachinery or helicopter rotors in which the flow is periodic. In this situation there is the opportunity to gain spectral accuracy by using a Fourier representation in time. During the last three years this idea has been investigated by McMullen, Jameson and Alonso,[5,6] and shown to provide dramatic reductions in computational time for periodic problems over previously used methods. A brief outline of the time-spectral method is given below.

Let $\hat{w}_k$ be the discrete Fourier transform of w^n,

$$\hat{w}_k = -\sum_{n=0}^{N} w^n e^{-ikn\Delta t}$$

Then the semi-discretization

$$\frac{dw}{dt} + R(w) = 0 \tag{3}$$

is discretized as the pseudo-spectral scheme

$$D_t w^n + R(w^n) = 0 \tag{4}$$

where

$$D_t w^n = \sum_{k=-\frac{N}{2}}^{\frac{N}{2}-1} ik\hat{w}_k e^{ikn\Delta t}$$

Here D_t is a central difference formula connecting all the time levels so equation (4) is an integrated space-time formulation which requires the simultaneous solution of the equations for all the time levels. Provided, however, that the solution is sufficiently smooth, equation (4) should yield spectral accuracy (exponential convergence with increasing N).

The time spectral equation (4) may be solved by dual time-stepping as

$$\frac{dw^n}{dt^*} + D_t w^n + R(w^n) = 0 \tag{5}$$

in pseudo-time t^*, as in the case of the BDF. Alternatively it may be solved in the frequency domain. In this case we represent equation (4) as

$$\hat{R}_k^* = ik\hat{w}_k + \hat{R}_k = 0 \tag{6}$$

where $\hat{R}_k$ is the Fourier transform of $R(w(t))$. Because $R(w)$ is nonlinear, $\hat{R}_k$ depends on all the modes $\hat{w}_k$. We now solve equation (6) by time evolution in pseudo-time

$$\frac{dw_k}{dt^*} + \hat{R}_k^* = 0 \tag{7}$$

At each iteration in pseudo-time $\hat{R}_k$ is evaluated indirectly. First $w(t)$ is obtained as the reverse transform of $\hat{w}_k$. Then we calculate the corresponding time history of the residual

$$R(t) = R(w(t))$$

and obtain $\hat{R}_k$ as the Fourier transform of $R(t)$, as shown in the diagram

While the time-spectral method should make it possible to achieve spectral accuracy, numerical tests have shown that it can give the accuracy required for practical applications ('engineering accuracy') with very small numbers of modes.

Incompressible Formulations based on Artificial Compressibility

While the above formulations have been primarily used in the context of compressible flows, in the limit of truly incompressible flow, or zero Mach number, alternative methods are needed to preserve the accuracy, robustness and convergence properties of the flow solution procedure. The fundamental difference between a compressible fluid model and an incompressible one is the loss of of the evolution equation for the density. Since the density is constant, a constraint must be imposed on the continuity equations to ensure a divergence-free velocity field. In addition, the eigenvalues resulting from the system of conventional hyperbolic Euler equations for compressible flows become infinite in the limit of incompressible flow. This is due to the fact that the sound speed becomes unbounded. Hence, the use of compressible flow solvers in the incompressible flow limit, introduces widely varying eigen speeds, resulting in extremely stiff equations. To overcome this difficulty, the present work uses the artificial compressibility method, an approach first proposed by Chorin in 1967[16] as a method to solve

viscous flows. Artificial compressibility methods introduce a psuedotemporal equation for the pressure through the continuity equation. This approach removes the troublesome sound waves associated with compressible flow formulations as the Mach number approaches zero. The eigenvalues of the original system are now replaced with an artificial set that renders the new set of equations well-conditioned for numerical computation. When combined with multigrid acceleration procedures, artificial compressibility proves to be particularly effective[17]. Converged solutions of incompressible flows over a main sail can be obtained in about 75-100 multigrid cycles.

Using the idea of artificial compressibility, the equations of motion of an incompressible, fluid can be cast in the following form:

$$\frac{\partial w}{\partial t} + P\left\{\frac{\partial F}{\partial x} + \frac{\partial G}{\partial y}\right\} = 0. \tag{8}$$

where w, f, g, h is the state and flux (inviscid and viscous) vectors and the preconditioning matrix P can be written as

$$P = \begin{bmatrix} \Gamma^2 & 0 & 0 & 0 \\ 0 & 1 & 0 & 0 \\ 0 & 0 & 1 & 0 \\ 0 & 0 & 0 & 1 \end{bmatrix}. \tag{9}$$

This set of equations has no physical meaning until the steady state is reached. At steady state, the time dependent pressure term drops from the continuity equation resulting in the true steady state equations for an incompressible flow. Further, Γ can be selected to accelerate the time decay to steady state.

Using the finite volume approach, the governing equations can be cast in the integral form for each computational volume in the domain as follows,

Conservation of Mass

$$\frac{d}{dt}\int_V p dV + \int_S \Gamma^2 (u \cdot n)\, dS = 0. \tag{10}$$

Conservation of Momentum

$$\frac{d}{dt}\int_V u dV + \int_S u(u \cdot n) dS = -\int_S p n dS, \tag{11}$$

Spatial discretization of equation (10) and (11) leads to a separate equation for each sub-domain in the computational mesh.

$$\frac{d}{dt} V_i w_i + \sum_k F_k . n_k S_k = 0, \tag{12}$$

where p is the pressure, u is the velocity vector, n is the unit normal at the surface of the control volume, V and S are the volume and surface area of the control volume respectively, F is the flux through the control volume and the summation of the fluxes is over the control volume that surrounds each node of the mesh.

Artificial Compressibility applied to the Time-Spectral Method

While the artificial compressibility method has been shown to be efficient for steady and unsteady simulations, it has not been previously explored for the time-spectral method.

Results

In the following sections, the relative merits and demerits of the four methods are discussed. Our benchmark test case is a NACA 0012 airfoil in plunge motion, with a plunge amplitude of 0.2 (times the chord) and a reduced frequency of 3.0. Unless otherwise reported the numerical method was stable for lower frequencies and/or plunge amplitudes.

Dual-Time Stepping

A NACA 0012 airfoil is simulated in plunge motion, with a plunge amplitude to chord ratio of 0.2, at a reduced frequency of 3.0. The reduced frequency is defined as $\omega\ chord/(2\ U_\infty)$. The meshes is of dimension, 512×64 and the simulations were performed in laminar mode. The Reynolds number for this simulation was 1800 and a Mach number of 0.2. Figure 1 shows the convergence history of the mean flow before the plunge cycle starts. Each time period was resolved with 72 time steps and the simulation was performed for 10 time periods to ensure that

a time periodic flow field was established. The Reynolds number for this simulation was 1800. Figures 3,4,5,6,7 shows the pressure distribution at various instances in the plunge cycle. Figure 2 shows the variation in the lift coefficient during the plunge cycle.

Time-Spectral

A NACA 0012 airfoil is simulated in plunge motion, with a plunge amplitude to chord ratio of 0.2, at a reduced frequency of 3.0. The reduced frequency is defined as $\omega\ chord/(2\ U_\infty)$. The meshes for all the methods are of dimension, 512×64 and the simulations were performed in laminar mode. Figure 8 shows the convergence history for the time-spectral approach. Figures 9,10,11,12 shows the pressure distribution at various instances of plunge cycle. This simulation was performed with 32 modes to resolve the temporally periodic flow-field. The Reynolds number for this simulation was 1000 and the Mach number was 0.2.

Artificial Compressibility

Artificial Compressibility for the Dual-time stepping Algorithm

The artificial compressibility correction was first implemented on the dual-time stepping algorithm. A NACA 0012 airfoil is simulated in plunge motion, with a plunge amplitude to chord ratio of 0.2, at a reduced frequency of 3.0. The reduced frequency is defined as $\omega\ chord/(2\ U_\infty)$. The meshes is of dimension, 512×64 and the simulations were performed in laminar mode. The Reynolds number for this simulation was 1800. Figure 13 shows the convergence history of the mean flow before the plunge cycle starts. Each time period was resolved with 72 time steps and the simulation was performed for 10 time periods to ensure that a time periodic flow field was established. The Reynolds number for this simulation was 1800. Figures 15,16,17,18,19 shows the pressure distribution at various instances in the plunge cycle. Figure 14 shows the variation in the lift coefficient during the plunge cycle.

Artificial Compressibility for the Time Spectral Algorithm

The artificial compressibility correction is now applied to the time spectral algorithm. The test case used here is the AGARD airfoil in pitching motion at a reduced frequency of 0.202 and pitch amplitude of 1 degree. This flow was simulated with 8 temporal modes. Figure 20 shows the convergence history. Figures 21,22 shows the pressure contours predicted by modes 1,4,8 and 12.

While the time spectral method in conjunction with the artificial comrpessibility correction can provide meaningful loading profiles for pitching/plunging airfoil calculations, when we applied to the test case that the other methods above were tested on, stability was a severe concern. For low reduced frequencies and/or plunge amplitudes, a small number of modes was sufficient to resolve the flow field. However, at higher frequencies even a large number of modes was insufficient to stabilize the calculation. An implicit formulation was also attempted to stabilize the computation without much success. The largest frequency/amplitude combination we were able to perform the computations was 0.2/0.08 with 32 modes and 300 Runge-Kutta cycles to converge each mode.

Conclusions

The numerical tests included in this study show that the implicit discretization driven by fast steady state solvers is adept at handling general unsteady flows. If the flow is temporally periodic and can be represented with a small number of modes, the time spectral method is a powerful approach. For the problems studied here, it is not conclusive if the time spectral method is the appropriate choice. The rich spectrum of harmonics that are present in the flows induced by the flapping motion suggest that the time-spectral method might require a large number of modes to resolve the flow field. The implicit discretization typically uses 72 instances in each time-period, with 25 inner iterations for each physical solution and 10 periods to resolve the flow field. This is approximately 18000 Runge-Kutta iterations to compute each flow field. The time-spectral method on the other hand uses an average of 36 modes and 500 Runge-Kutta iterations each to obtain the time harmonic solution. This also leads to approximately 18000 Runge-Kutta iterations. With artificial compressibility, the implicit discretization is stable across a range of reduced frequencies and plunge amplitudes while the time spectral approach on the other hand is less stable (even with larger number of modes) for high frequency plunge motions. The computational cost coupled with robustness makes us believe that the implicit discretization is the more appropriate choice of numnerical method for flapping wing simulations.

References

[1]Lighthill, J. Mathematical Biofluidynamics Regional Conference Series in Applied Mathematics Siam, 1975.

[2]Weis-Fogh T. and Jensen M. Proceedings of the Royal Soceity B. 239, pp. 415-584, 1956.

[3]Ellington, C.P., Van Der Berg C, Willmott, A.P. and Thomas, A.L.R. Leading-edge vortices in insect flight, Nature, 384, 626-630.

[4]Dickinson, M.H., Lehmann, F., Sane, S.P. Wing Rotation and the Aerodynamics basis of insect flight American Zoologist, 38, 718-728.

[5], M. McMullen, A. Jameson and J.J. Alonso, Acceleration of Convergence to a Periodic Steady State in Turbomachinery Flows AIAA 39th Aerospace Sciences Meeting, 01-0152, Reno, NV, 2001.

[6], M. McMullen, A. Jameson and J.J. Alonso, Application of a Non-Linear Frequency Domain Solver to the Euler and Navier-Stokes Equations AIAA 40th Aerospace Sciences Meeting and Exhibit, 02-0120, Reno, NV, 2002.

[7], Gopinath, A, Efficient Fourier-Based Algorithms for Time-Periodic Unsteady Problems, Phd. thesis, Department of Aeronautics and Astronautics, Stanford University, 2007.

[8]A. Jameson. Optimum Aerodynamic Design Using Control Theory Computational Fluid Dynamics Review 1995 Wiley, 1995.

[9]A. Jameson. Time dependent calculations using multigrid, with applications to unsteady flows past airfoils and wings. *AIAA paper 91-1596*, AIAA 10th Computational Fluid Dynamics Conference, Honolulu, Hawaii, June 1991.

[10]G. Dahlquist. A special stability problem for linear multistep methods. *BIT*, 3:27–43, 1963.

[11]C.W. Gear. The numerical integration of stiff ordinary differential equations. Report 221, University of Illinois Department of Computer Science, 1967.

[12]N. D. Melson, M. D. Sanetrik, and H. L. Atkins. Time-accurate Navier-Stokes calculations with multigrid acceleration. In *Proceedings of the Sixth Copper Mountain Conference on Multigrid Methods*, Copper Mountain, April 1993.

[13]J. J. Alonso and A. Jameson. Fully-implicit time-marching aeroelastic solutions. *AIAA paper 94-0056*, AIAA 32nd Aerospace Sciences Meeting, Reno, NV, January 1994.

[14]J. J. Alonso, L. Martinelli, and A. Jameson. Multigrid unsteady Navier-Stokes calculations with aeroelastic applications. *AIAA paper 95-0048*, AIAA 33rd Aerospace Sciences Meeting, Reno, NV, January 1995.

[15]A. Belov, L. Martinelli, and A. Jameson. A new implicit algorithm with multigrid for unsteady incompressible flow calculations. *AIAA paper 95-0049*, AIAA 33rd Aerospace Sciences Meeting, Reno, NV, January 1995.

[16]A. Chorin, A Numerical Method for Solving the Incompressible Viscous Flow problem, *Journal of Computational Physics* Vol. 2, pp 12-26, 1967.

[17]J. Farmer, L. Martinelli and A. Jameson, A Fast Multigrid Method for Solving Incompressible Hydrodynamic Problems with Free Surfaces, *AIAA Paper 93-0767*, 31^{st} AIAA Aerospace Sciences Meeting, Reno, January, 1993.

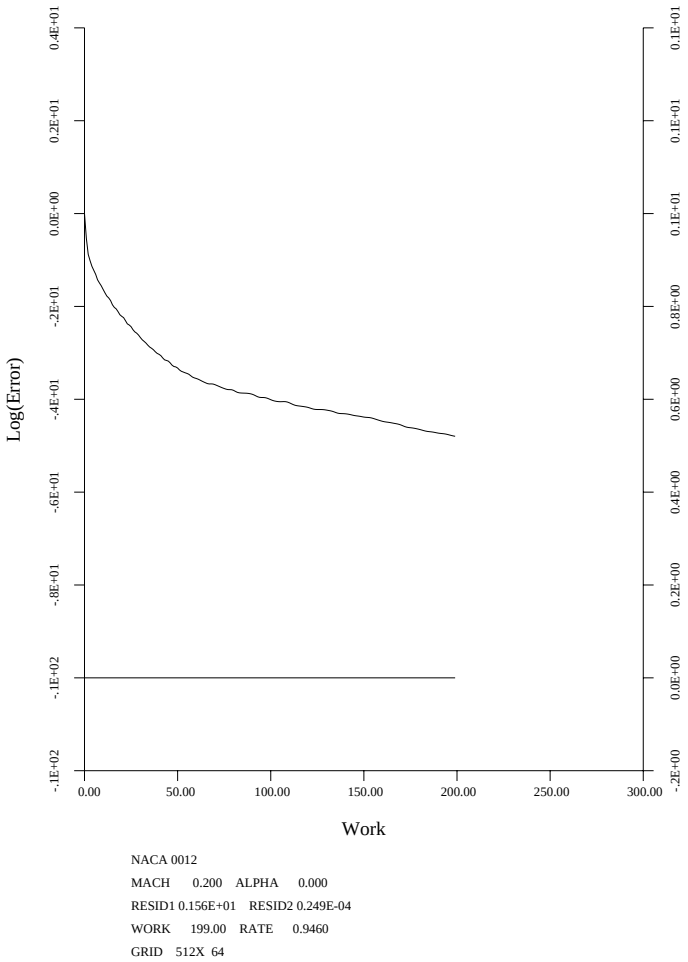

Fig. 1 Convergence history for the Dual-Time Stepping Method

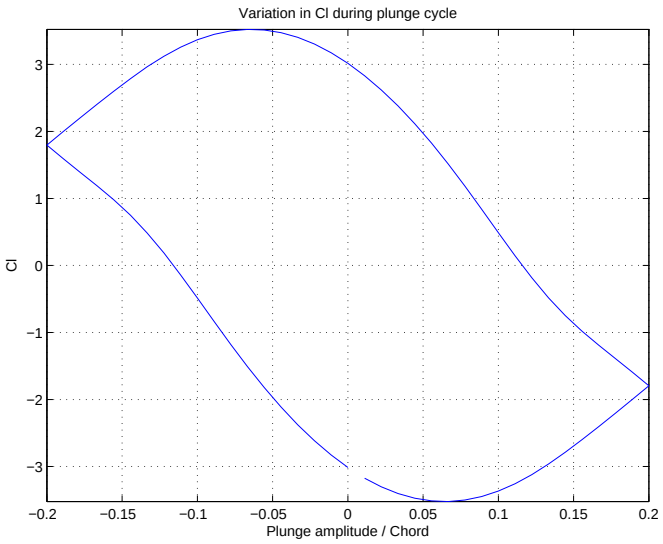

Fig. 2 Variation in Cl during the plunge cycle

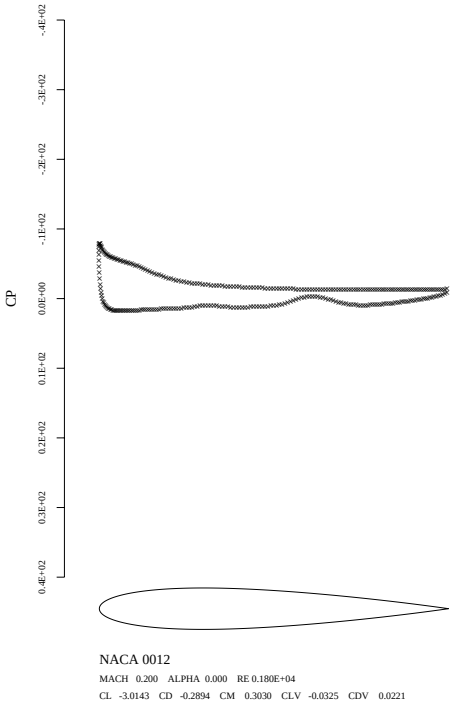

a) t=0

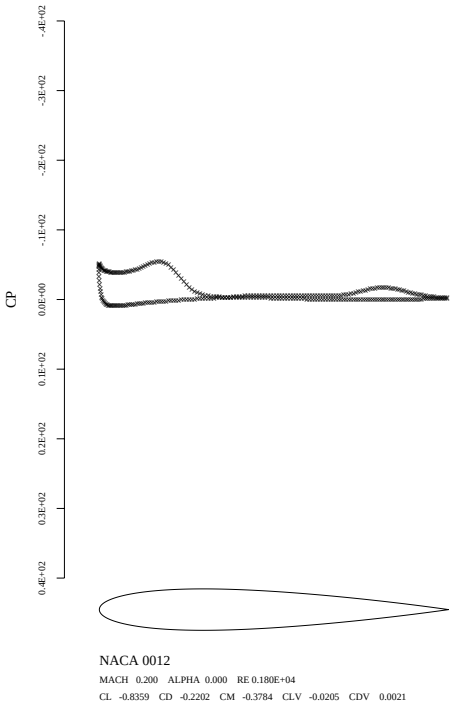

b) t=T/10

Fig. 3 Pressure Distribution at various instances in the plunge cycle

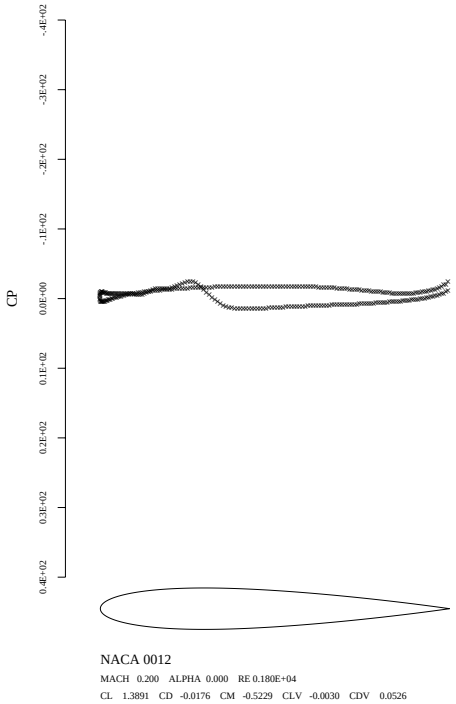

a) t=2T/10

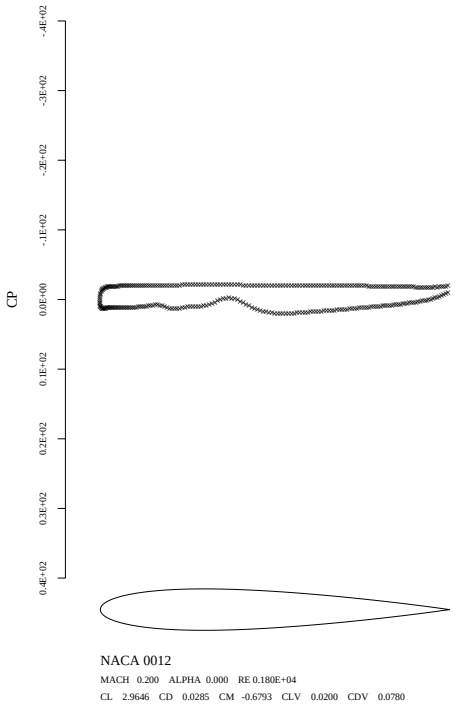

b) t=3T/10

Fig. 4 Pressure Distribution at various instances in the plunge cycle

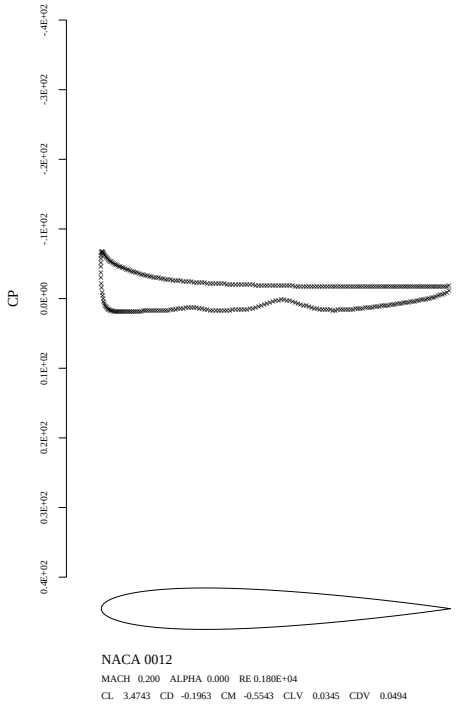

a) t=4T/10

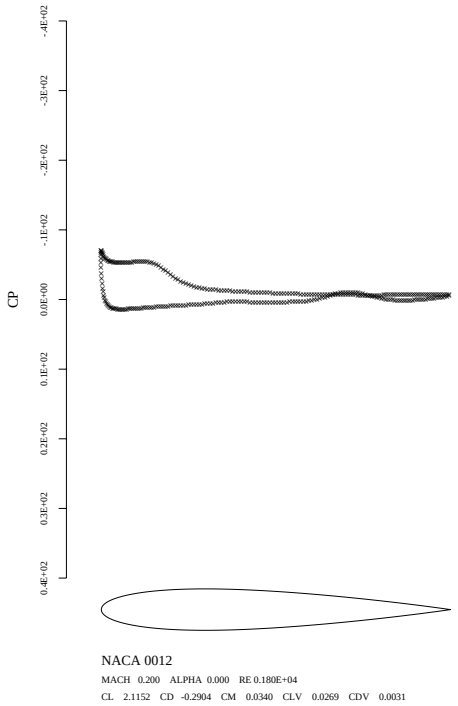

b) t=5T/10

Fig. 5 Pressure Distribution at various instances in the plunge cycle

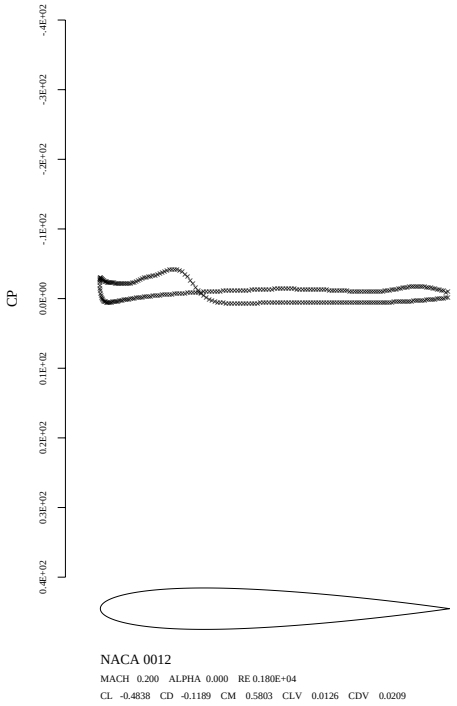

a) t=6T/10

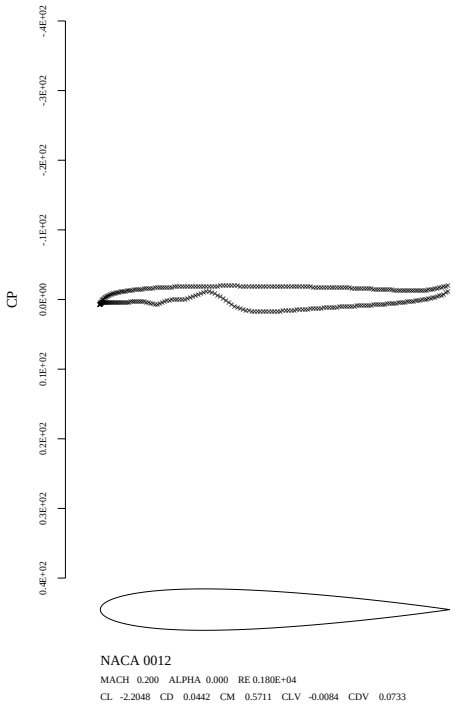

b) t=7T/10

Fig. 6 Pressure Distribution at various instances in the plunge cycle

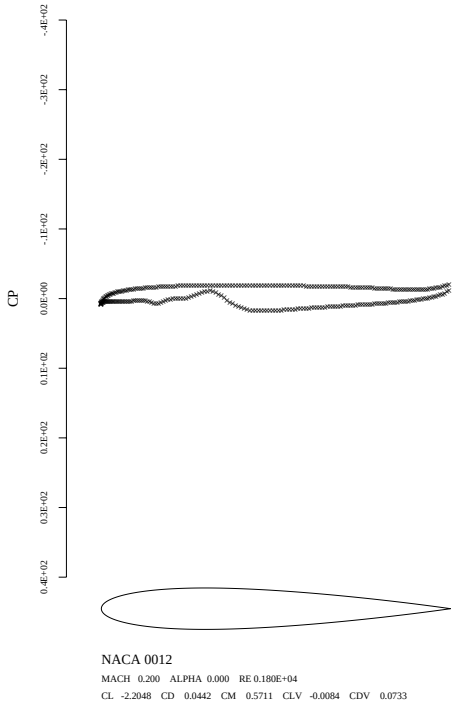

a) t=8T/10

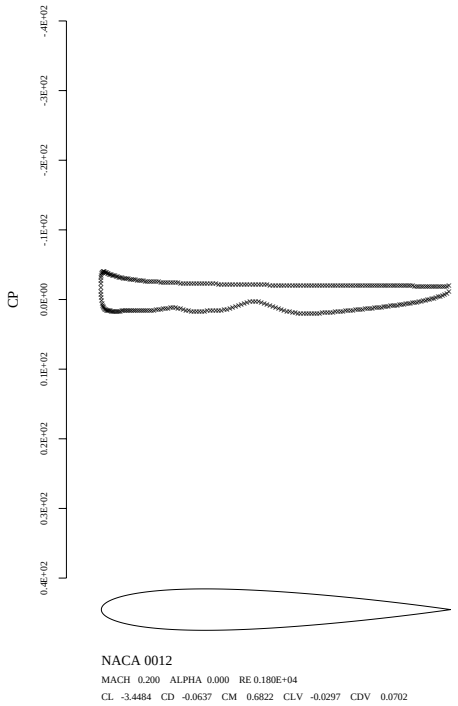

b) t=9T/10

Fig. 7 Pressure Distribution at various instances in the plunge cycle

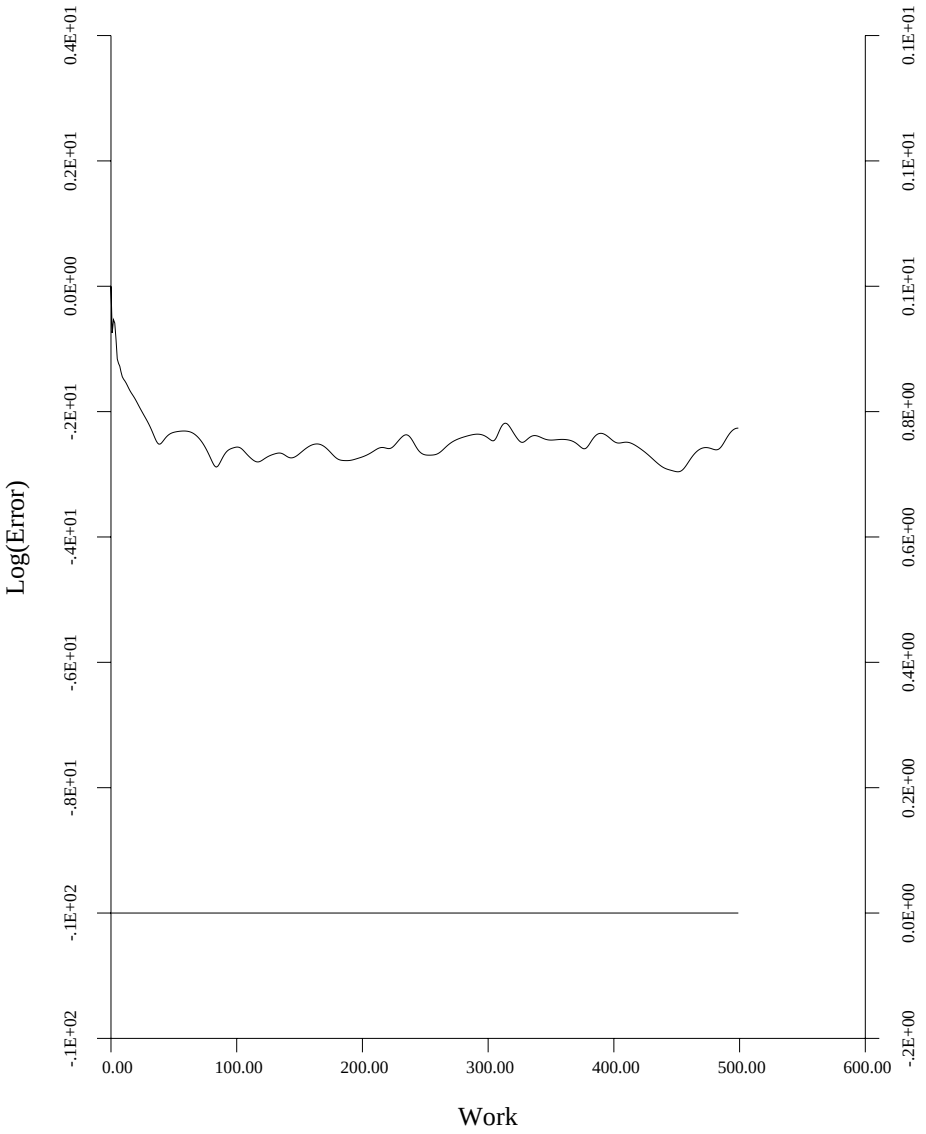

Fig. 8 Convergence history for the Time-Spectral Method

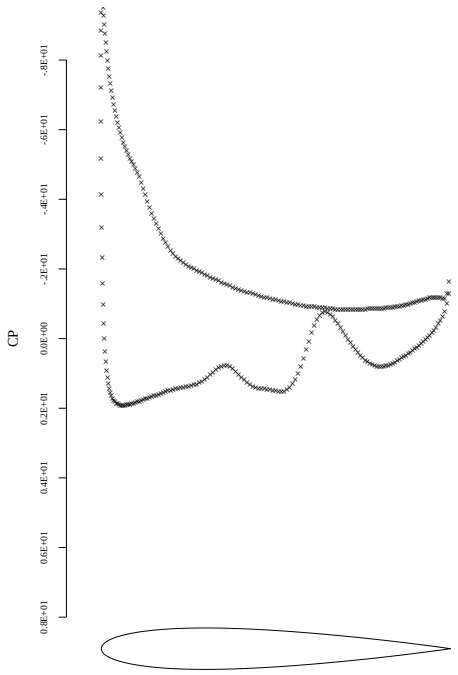

a)

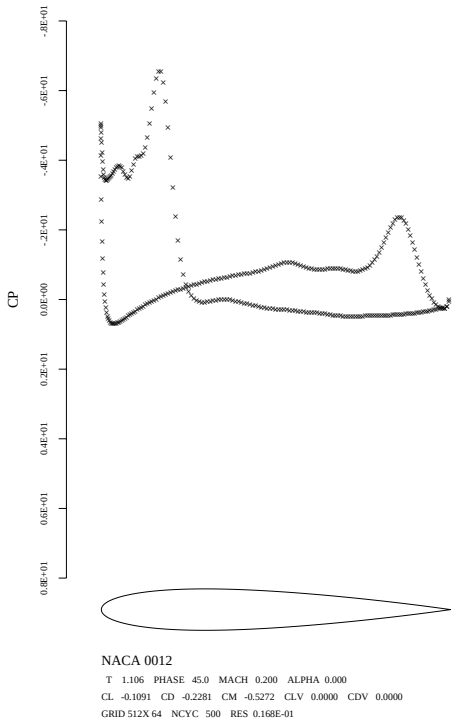

b)

Fig. 9 Pressure Distribution at various instances in the plunge cycle

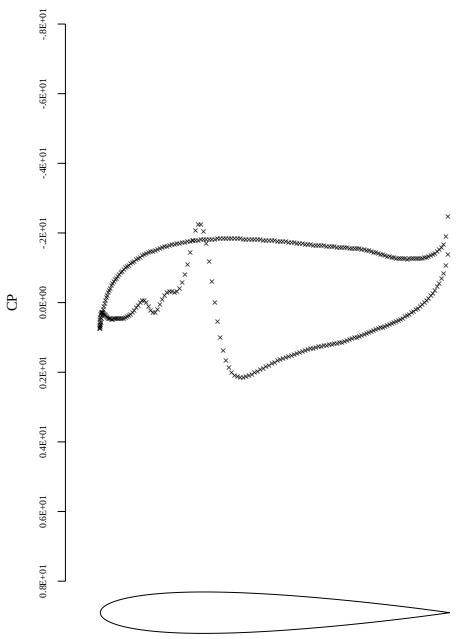

a)

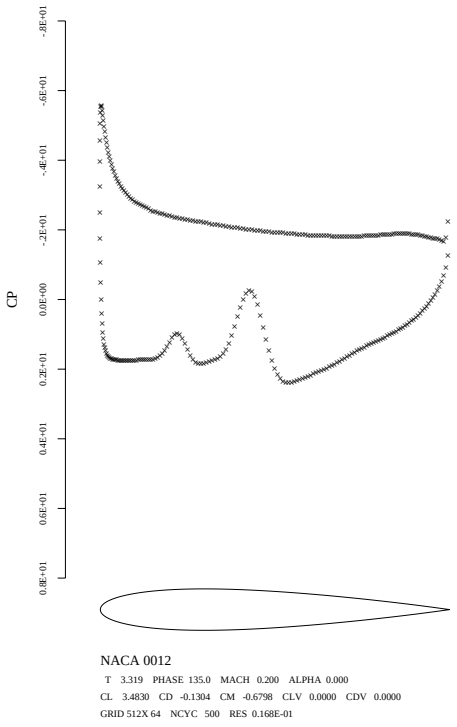

b)

Fig. 10 Pressure Distribution at various instances in the plunge cycle

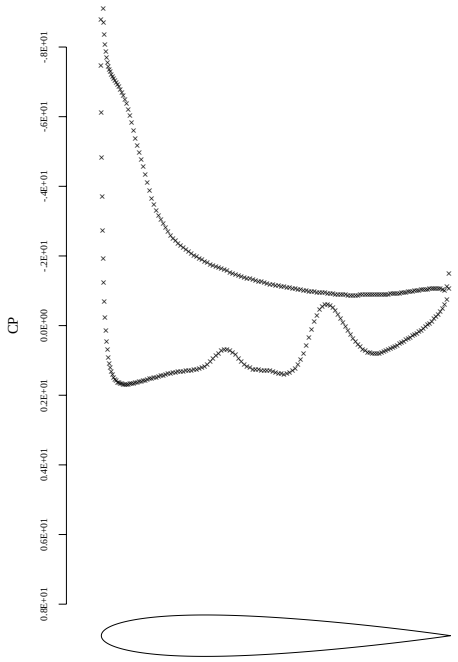

a)

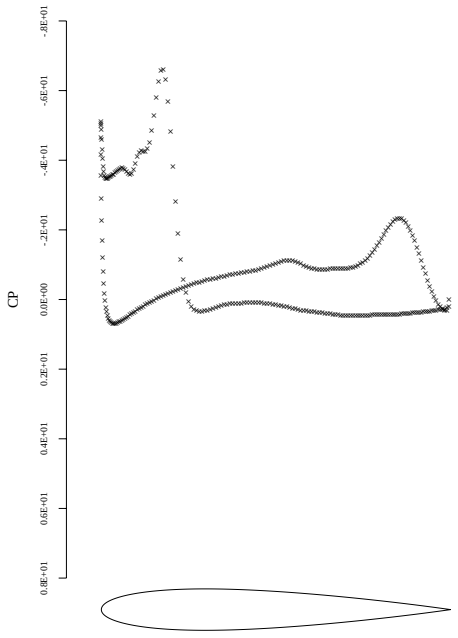

b)

Fig. 11 Pressure Distribution at various instances in the plunge cycle

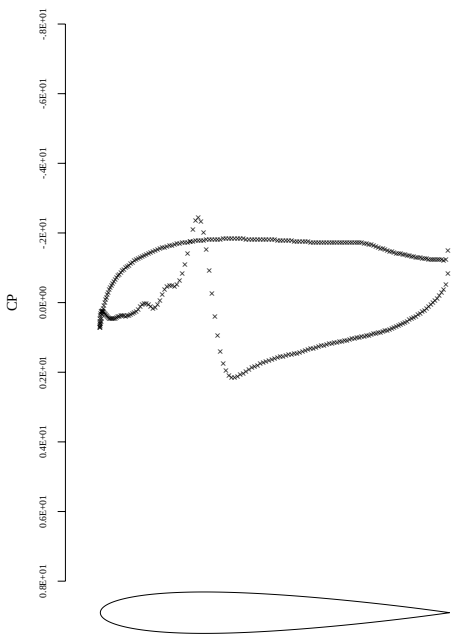

a)

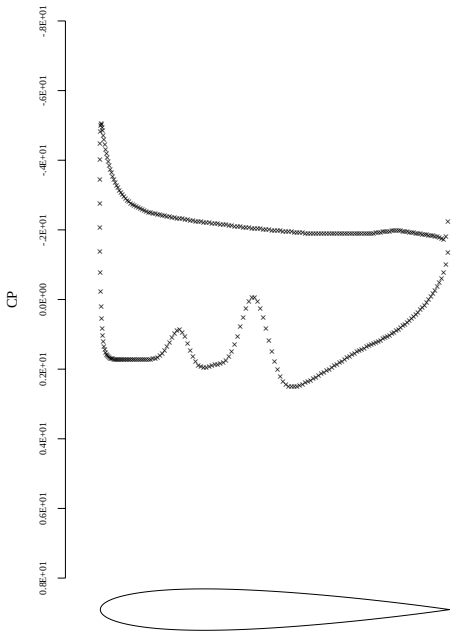

b)

Fig. 12 Pressure Distribution at various instances in the plunge cycle

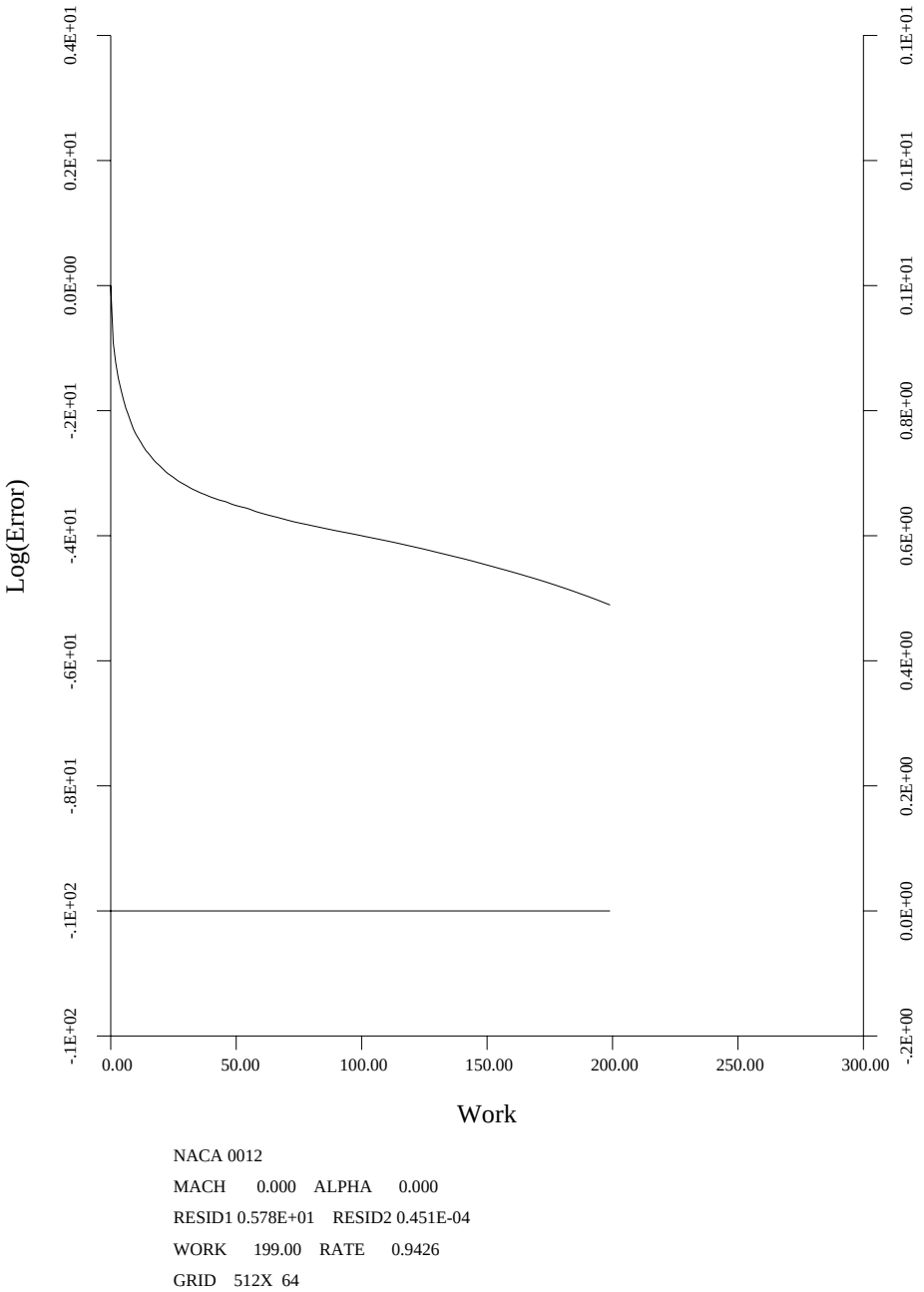

Fig. 13 Convergence history for the Dual-Time Stepping Method with artificial compressibility

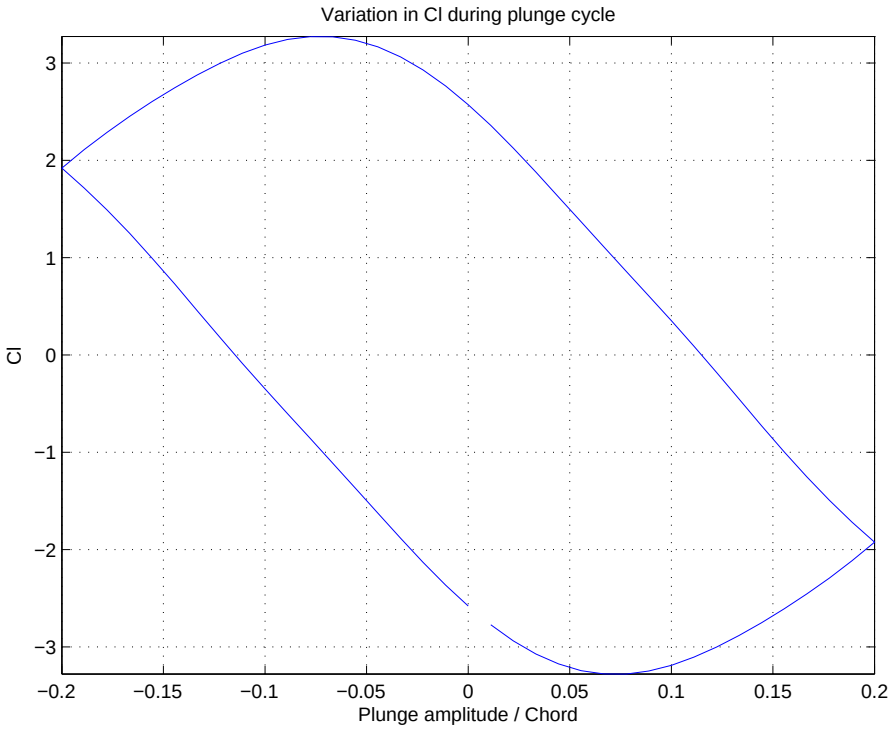

Fig. 14 Variation in Cl during the plunge cycle

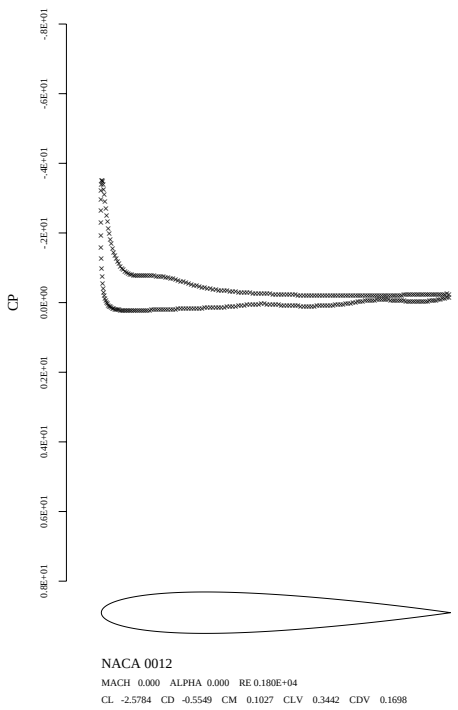

a) t=0

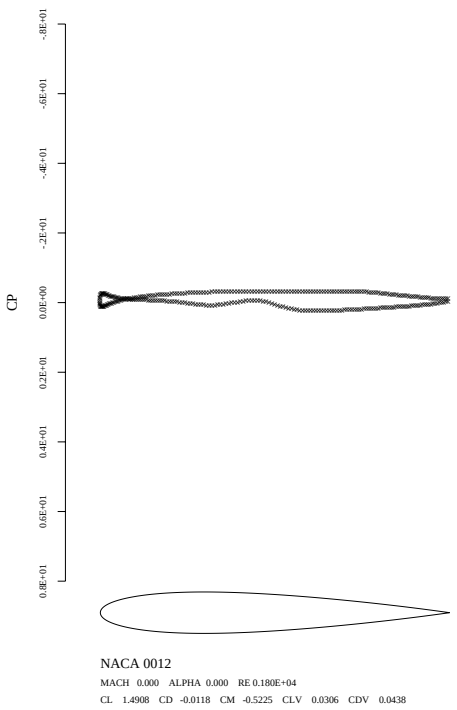

a) t=2T/10

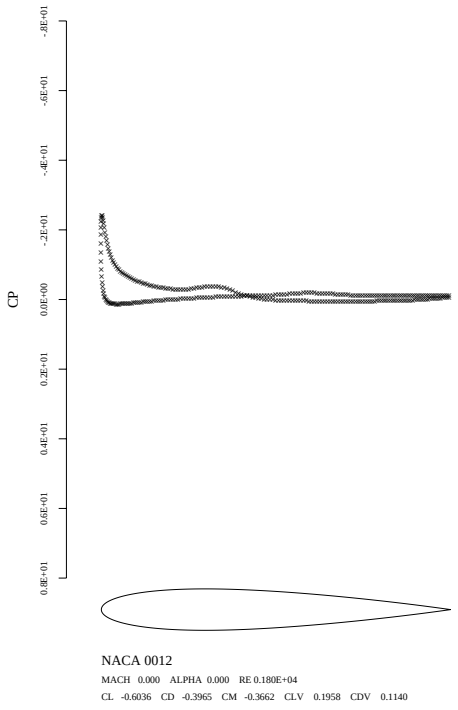

b) t=T/10

Fig. 15 Pressure Distribution at various instances in the plunge cycle

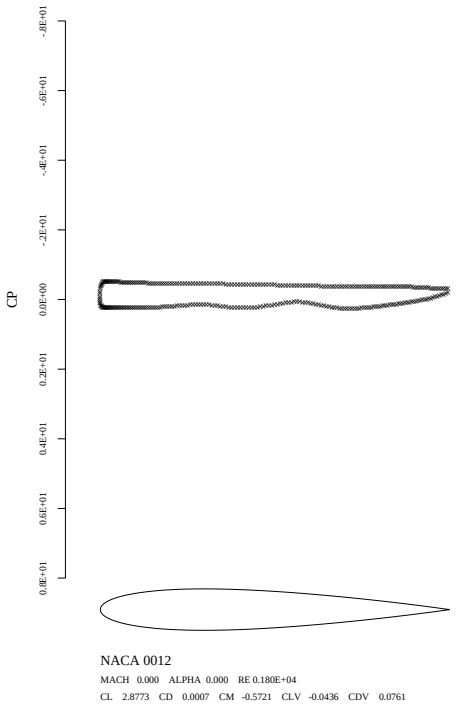

b) t=3T/10

Fig. 16 Pressure Distribution at various instances in the plunge cycle

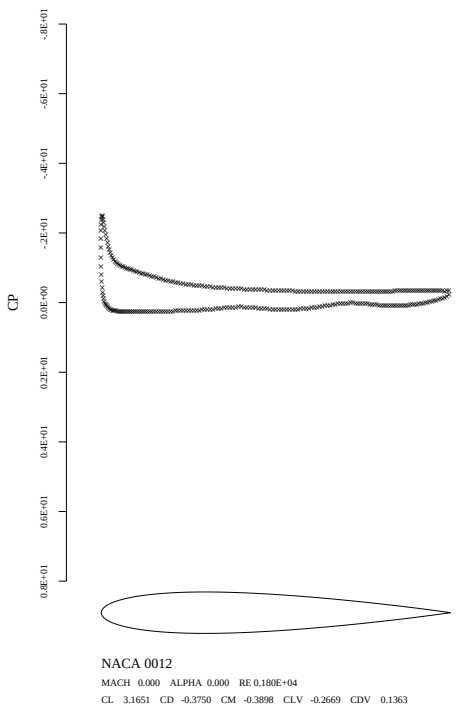

a) t=4T/10

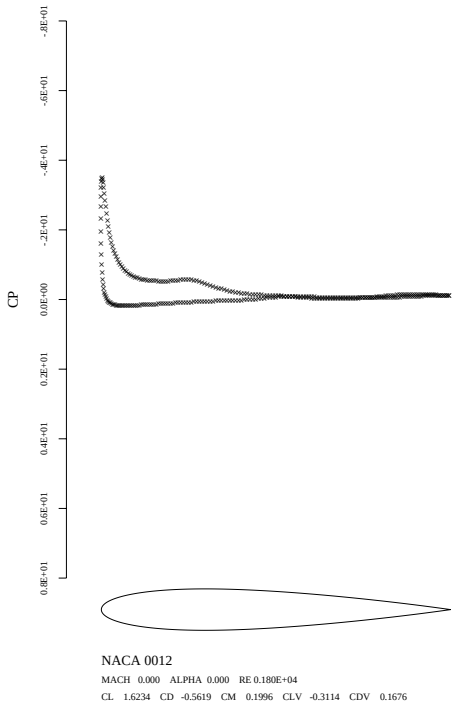

b) t=5T/10

Fig. 17 Pressure Distribution at various instances in the plunge cycle

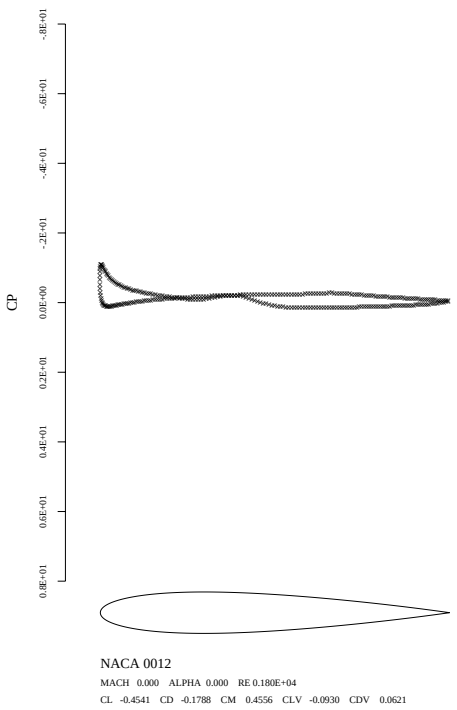

a) t=6T/10

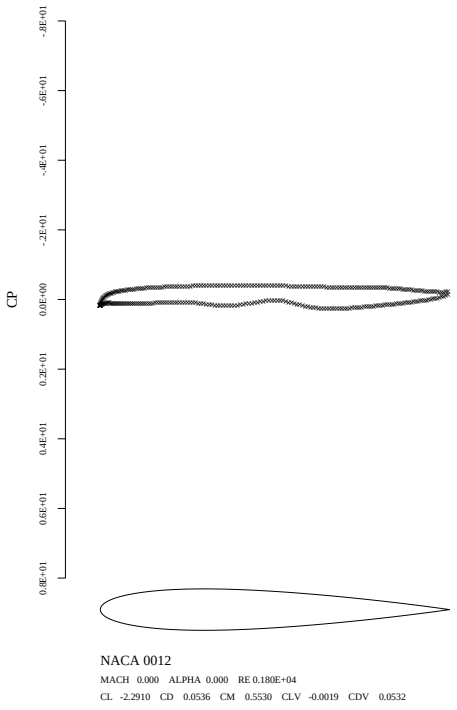

b) t=7T/10

Fig. 18 Pressure Distribution at various instances in the plunge cycle

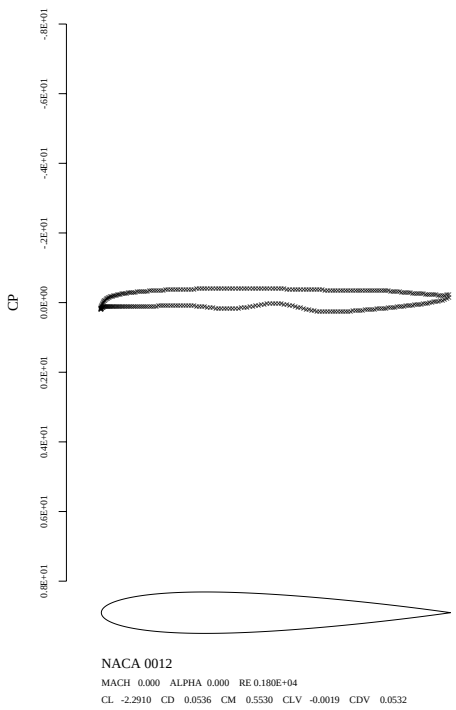

a) t=8T/10

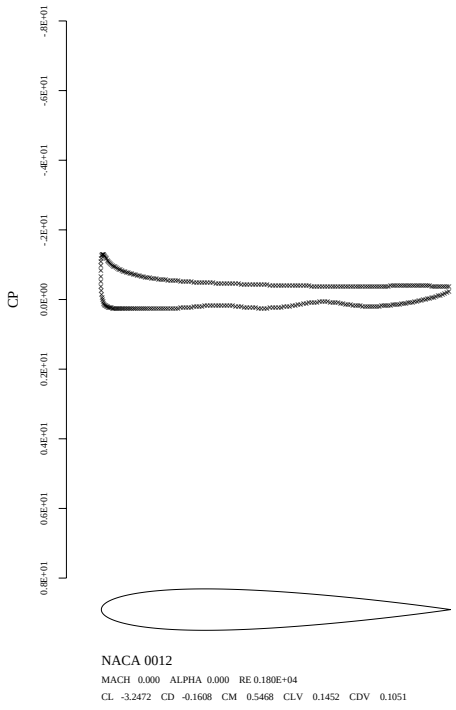

b) t=9T/10

Fig. 19 Pressure Distribution at various instances in the plunge cycle

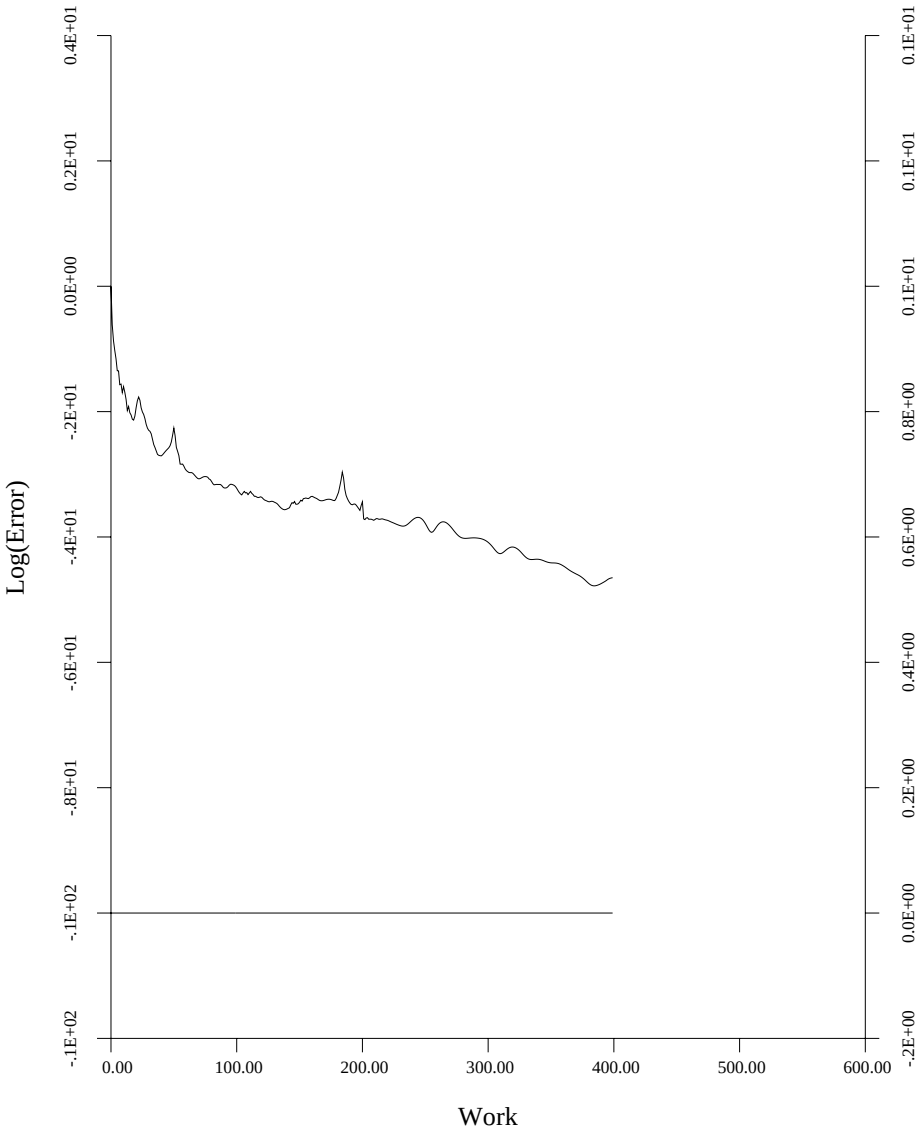

Fig. 20 Convergence history for the time spectral method with artificial compressibility

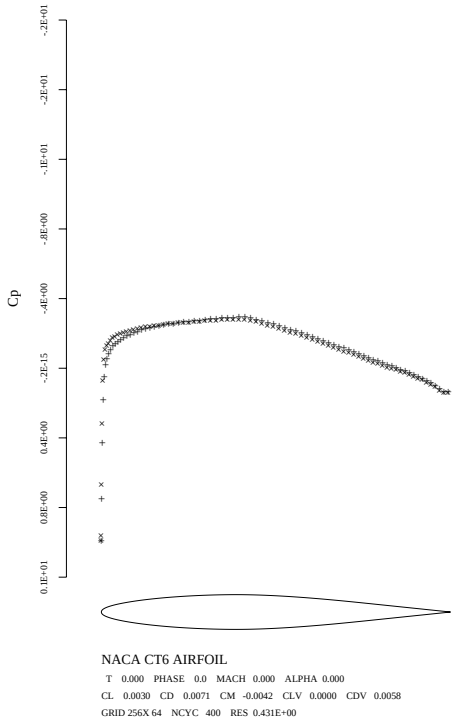

a) t =0

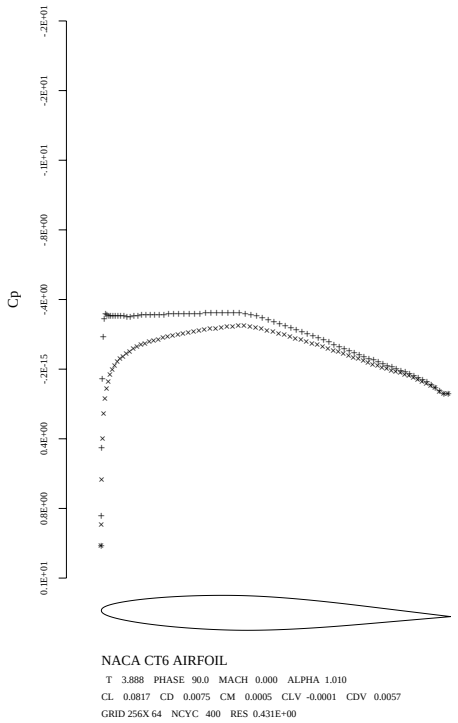

b) t =T/4

Fig. 21 Pressure Distribution at various instances in the plunge cycle

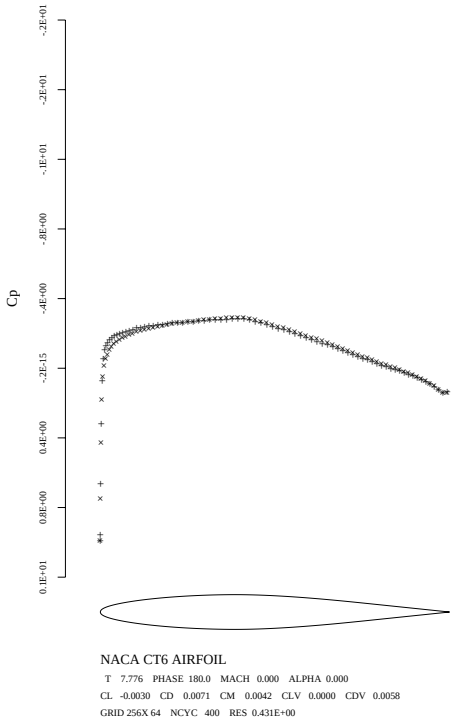

a) t=T/2

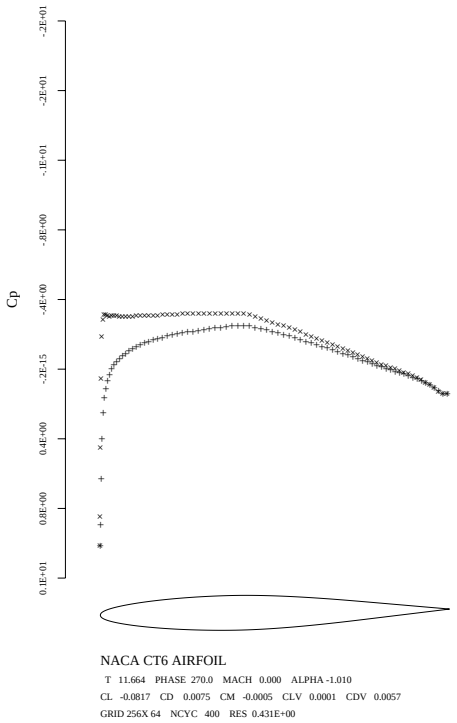

b) t=3T/4

Fig. 22 Pressure Distribution at various instances in the plunge cycle